IOPscience iopscience.iop.org

Home Search Collections Journals About Contact us My IOPscience

An x-ray spectroscopic study of A_2FeMoO_6 and $Sr_2Fe_{1-x}Cr_xMoO_6$ double perovskites

This article has been downloaded from IOPscience. Please scroll down to see the full text article.

2004 J. Phys.: Condens. Matter 16 6877

(http://iopscience.iop.org/0953-8984/16/39/020)

View the table of contents for this issue, or go to the journal homepage for more

Download details:
IP Address: 129.252.86.83
The article was downloaded on 27/05/2010 at 17:58

Please note that terms and conditions apply.

INSTITUTE OF PHYSICS PUBLISHING JOURNAL OF PHYSICS: CONDENSED MATTER

J. Phys.: Condens. Matter **16** (2004) 6877–6890 PII: S0953-8984(04)77300-2

An x-ray spectroscopic study of A_2FeMoO_6 and $Sr_2Fe_{1-x}Cr_xMoO_6$ double perovskites

J Herrero-Martín, J García, G Subías, J Blasco[1] and M C Sánchez

Instituto de Ciencia de Materiales de Aragón and Departamento de Física de la Materia Condensada, CSIC-Universidad de Zaragoza, C/Pedro Cerbuna, 12, 50009 Zaragoza, Spain

E-mail: jbc@unizar.es

Received 3 March 2004
Published 17 September 2004
Online at stacks.iop.org/JPhysCM/16/6877
doi:10.1088/0953-8984/16/39/020

Abstract

The electronic and geometrical local structures of A_2FeMoO_6 (A = Ca, Sr, Ba, $Ba_{1/2}Sr_{1/2}$) and $Sr_2Fe_{1-x}Cr_xMoO_6$ ($x = 0, 1/4, 1/2, 3/4, 1$) compounds have been investigated by means of x-ray absorption spectroscopy at the iron, chromium and molybdenum K edges. The Mo K-edge spectra show a similar electronic state for Mo in all samples with similar Mo–O distances. At the Fe K edge, instead, XANES and EXAFS spectra showed significant differences along the A_2FeMoO_6 series, denoting an influence of the divalent A metal in the electronic state of iron. Both the chemical shift at the iron K edge and the interatomic Fe–O distances closely correspond to Fe^{3+} for Sr_2FeMoO_6 and Ca_2FeMoO_6 while a mixed valence state (between +2 and +3) is deduced for the Ba samples. We have not observed differences in the spectra of the $Sr_2Fe_{1-x}Cr_xMoO_6$ series for any of the absorption edges. This demonstrates that substitution of Fe with Cr is homovalent. Our work suggests that the description in terms of a band model is a better approximation than an ionic model.

(Some figures in this article are in colour only in the electronic version)

1. Introduction

The double-perovskite compounds $A_2BB'O_6$ (A = Ba, Sr, Ca) have recently attracted scientific and technological interest due to the discovery of tunnelling magnetoresistance at room temperature [1]. Different B and B′ cations occupy the perovskite B sites alternatively. The double perovskites with BB′ = FeMo, FeRe, CrRe etc, are magnets with a Curie temperature above room temperature. For instance, A_2FeMoO_6 samples have T_C ranging [2] between 330 and 420 K. The lowest T_C corresponds to the Ba_2FeMoO_6 compound that shows the largest

[1] Author to whom any correspondence should be addressed.

 © 2004 IOP Publishing Ltd Printed in the UK

crystallographic cell with cubic symmetry [3]. The replacing of Ba with smaller cations leads to a diminution of the unit cell size together with a lowering of the crystal symmetry. In this way, Sr_2FeMoO_6 has the highest T_C and a tetragonal cell [3, 4], while Ca_2FeMoO_6 crystallizes in a monoclinic cell [3, 5] and its T_C is a bit lower showing a competition effect between cell volume and structural distortion. The decrease of the former tends to increase the magnetic interaction whereas the increase of the latter leads to a decrease of the Fe–O–Mo bond angle diminishing the magnetic interaction (either superexchange or double exchange). Amazingly, this competition effect does not exist in A_2FeReO_6 compounds [6] where the insulating and monoclinic Ca_2FeReO_6 shows the highest T_C in the series, i.e. the volume decrease overcomes the distortion effect in this case.

The magnetic ordering and relevant magnetic interactions in the A_2FeMoO_6 double perovskites is a matter of controversy. Band calculations [1] proposed a half-metallic ground state due to antiferromagnetic coupling between localized Fe^{3+} and the single itinerant downspin electron provided by the Mo^{5+}. However, later studies suggest that the physical properties strongly depend on the 2p(O)–4d(Mo) hybridization [7]. Neutron scattering experiments showed a ferromagnetic ordering of the iron sublattice for these samples but the existence of localized magnetic moment on the molybdenum atom is not well established. It seems to depend on the compound and it is also very likely to depend on synthesis details. For example, neutron diffraction determined 0.7 μ_B for Mo, antiferromagnetically coupled to Fe, in Ca_2FeMoO_6, whereas a negligible value was observed for Ba_2FeMoO_6 [3]. Controversies between experimental and theoretical magnetic moments have also been reported. Several authors ascribed this discrepancy to a miss-site defect in the ordered B–B′ arrangement [1, 8] whereas other works emphasized the role of cationic vacancies [3, 4]. In general, mixed oxides are described in the frame of the ionic model, i.e. using integer ionic states. Therefore, the first task is to deduce the best ionic model for this system. Two couples can be inferred, either Fe^{3+}–Mo^{5+} or Fe^{2+}–Mo^{6+}. Localized magnetic moment on the Mo site could only be detected for the first couple (Mo^{5+}, $4d^1$). Historically, the ferrimagnetism in these double perovskites has been explained as due to antiferromagnetic superexchange interaction between $Mo^{5+}(5d^1)$ and the $Fe^{3+}(3d^5)$ spins [9, 10]. In the second case, the presence of $Mo^{6+}(4d^0)$ without local magnetic moment implies the ferromagnetic ordering of the iron sublattice. The second task is to verify whether an ionic model is valid for this system or whether its properties are better explained in terms of an intermediate valence as suggested by several authors [11, 12].

One concludes the necessity of an accurate knowledge of the metal electronic states to gain insight into both the conduction mechanism and the magnetic interactions. Previous attempts to ascertain the atomic electronic state of Mo and Fe gave rise to serious controversies. In this way, while some x-ray magnetic circular dichroism data did not show any observable spin magnetic moment on Mo in the Sr_2FeMoO_6 [13], other authors reported instead a measurable moment of -0.32 μ_B confirming the ferrimagnetic ordering [14]. The Fe valence was also the subject of contradictory results. X-ray absorption spectroscopy data of Sr_2FeMoO_6 at the Fe L edge either conclude that iron is in the +3 state [13] or in an intermediate valence Fe^{2+}/Fe^{3+} [14, 15]. Furthermore, Mössbauer experiments were also interpreted in terms of Fe^{3+} [16] or in terms of Fe^{2+}/Fe^{3+} [17]. Accordingly, the oxidation state for Fe and Mo in these compounds is not well understood so far.

In order to shed light on the valence of Fe and Mo, we have used XANES (x-ray absorption near edge structure) spectroscopy at the iron and molybdenum K edges in the A_2FeMoO_6 series (A = Ba, $Ba_{1/2}Sr_{1/2}$, Sr and Ca). This study will allow us to determine the accuracy of an ionic model for this system—i.e. the value of integer valence—and whether the valences are alike for all compounds or there is any relationship between valence and localized magnetic moment on Mo atoms.

We have also performed EXAFS spectra in order to determine the interatomic Fe–O and Mo–O distances along the series for the sake of comparison with the data obtained from diffraction techniques. The correlation between the valence and the interatomic distance [18] should support the XANES results. In addition, synthesis details are very important. We have realized that the usual synthesis procedure leads to the formation of tiny impurities of α-Fe. These impurities affect the analysis at the Fe K edge of these compounds. Therefore, we were forced to test alternative synthesis routes in order to minimize this undesirable effect.

In order to gain insight into the factors that control the magnetic and conduction properties in this kind of compounds, we have also studied the electronic and geometrical local structure of $Sr_2Fe_{1-x}Cr_xMoO_6$ samples. In this case, we keep the A atom fixed and dope the B site. Sr_2CrMoO_6 is closely related to Sr_2FeMoO_6. Both have a ferrimagnetic ground state and the same crystallographic structure. However, electronic conduction is quite different. The Cr sample is semiconducting at low temperatures while the Fe compound becomes metallic in the ferrimagnetic state [19, 20]. Moreover, defects such as oxygen vacancies or miss-site disorder are higher for the Cr compound [20]. Therefore, it is also interesting to determine how these defects affect the electronic state of the constituent atoms in order to account for the different physical properties.

The paper follows this scheme: first, we study the effect of preparation method on the EXAFS and XANES spectra of the series A_2FeMoO_6. Second, a complete XAS study of pure A_2FeMoO_6 samples was done. Finally, we present the XAS study of the $Sr_2Fe_{1-x}Cr_xMoO_6$ samples and a brief discussion with the main conclusions of this work.

2. Experimental and data analysis

Two sets of A_2FeMoO_6 samples were prepared following two synthesis routes. The synthesis of the first set (hereafter denoted as set A) is reported elsewhere [3]. It is noteworthy that this route is widely used by the scientific community [21–23]. Briefly, stoichiometric amounts of ACO_3, Fe_2O_3 and MoO_3 were mixed, ground and calcined at 900 °C for 2 h and then sintered at 1200 °C for 24 h in a current flow of H_2/Ar (2/98) with intermediate grindings. Tiny amounts of α-Fe are observed in some of the x-ray patterns. Structural characterization and physical properties were also reported in [3]. The second set (set B) was also prepared by solid state reaction, but in this case stoichiometric amounts of $BaCO_3$, $SrCO_3$, $CaCO_3$, Fe_2O_3, 2/3 MoO_3 and 1/3 Mo were mixed, ground, pressed into pellets and heated at 1200 °C for 4 h in a pure atmosphere of Ar. The Mo:MoO_3 ratio is higher than the theoretical one (1/6:5/6) to compensate further oxidation. This step is enough to form the Ca_2FeMoO_6 sample with minor impurities of CaO. The other samples, instead, contained a significant amount of secondary phases such as $AMoO_4$ (A = Ba, Sr). In order to remove the secondary phases, the samples were ground, pressed and sintered at 1200 °C in a stream of H_2/Ar (2/98) for 1 h. We note that this short sintering time in reducing conditions prevents the segregation of Fe. The samples were characterized by x-ray powder diffraction using a D-max Rigaku system with a Cu rotating anode. The B samples were single phases with no α-Fe detected in their patterns.

Finally, $Sr_2Fe_{1-x}Cr_xMoO_6$ are prepared from stoichiometric amounts of $SrCO_3$, Fe_2O_3, Cr_2O_3 and MoO_3. They were mixed, ground and calcined at 900 °C for 2 h and then sintered at 1250 °C for 8 h in reducing conditions (as for set A of samples). The full characterization of the samples is reported in [19]. Shorter sintering times did not give a pure final product, while more time leads to the presence of α-Fe, so 8 h was a compromise between both factors. Nevertheless, the very tiny amounts of α-Fe allow us to perform the spectroscopic analysis.

The x-ray absorption experiments were carried out in transmission mode at the beamline BM29, ESRF, Grenoble (France). The storage ring operating conditions were 6 GeV electron

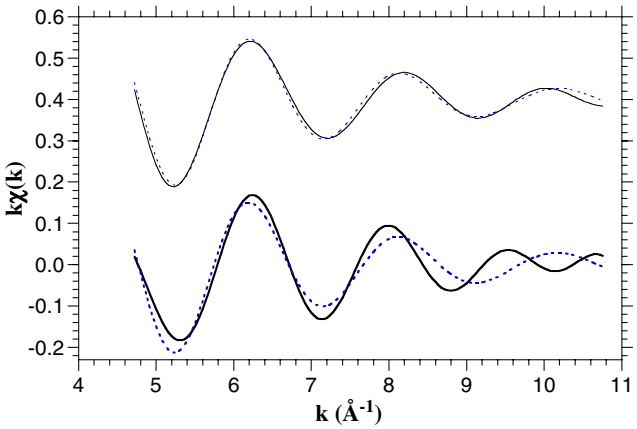

Figure 1. EXAFS signal (continuous curve) and best fit (dotted curve) of the Fourier filtered first shell using oxygen scatters for (bottom) set A of Ca_2FeMoO_6 and (top) set B of Ca_2FeMoO_6. The Fourier transform (FT) of the $k\chi(k)$ spectra was extracted using a Gaussian window between 4.5 and 11 $Å^{-1}$. The first-shell contribution was extracted by Fourier filtering of the FT spectra between 0.8 and 2.3 Å.

energy and 150–190 mA electron current. A Si(311) double-crystal monochromator was used for Fe K-edge and Mo K-edge measurements. The incident and transmitted beams were detected by means of ionization chambers. The energy resolution $\delta E/E$ was estimated to be about 6×10^{-5}. The spectra were collected at 30 K using a closed-cycle helium cryostat whose accuracy was estimated to be ± 1 K.

XANES spectra were normalized to the high-energy part of the spectrum ($\sim$100 eV) after background subtraction. The experimental EXAFS signal was extracted from the raw spectra following standard methods [24]. Background removal was performed and the atomic absorption coefficient was determined by a low-order polynomial fit of the spectra. The structural analysis was mainly restricted to the first coordination shell except for the A_2FeMoO_6 samples where a two-shell analysis was performed up to 4.5 Å. In both cases, we have used the theoretical phases and amplitudes provided by the FEFF 8.10 code [25]. Such phases and amplitudes were verified by fitting some reference compounds ($LaFeO_3$ or $SrMoO_3$). The agreement with crystallographic data turned out to be excellent.

3. Results

3.1. A_2FeMoO_6 series

First, we are going to point out the influence of α-Fe contamination in the EXAFS spectra of these compounds. For the sake of comparison, we show the Fourier filtered first-shell EXAFS spectra of the Fe K edge for both samples—sets A and B—of Ca_2FeMoO_6 in figure 1. It is worth observing that the scattering amplitude at relatively high wavevector (k) is higher for sample A. Such a large amplitude is not expected from the scattering of oxygen atoms, indicating an additional contribution from heavier atoms to the first shell. Our attempts to fit the A-sample spectrum considering only the oxygen coordination shell were unsuccessful as displayed in the bottom of figure 1. This is also true for the rest of the A samples.

In order to account for this result, we reanalysed the quality of our samples. Figure 2 shows the x-ray pattern of the $BaSrFeMoO_6$ (set A). As mentioned, we have detected tiny impurities of α-Fe (better noticed in the inset of figure 2). We have performed Rietveld analysis of the

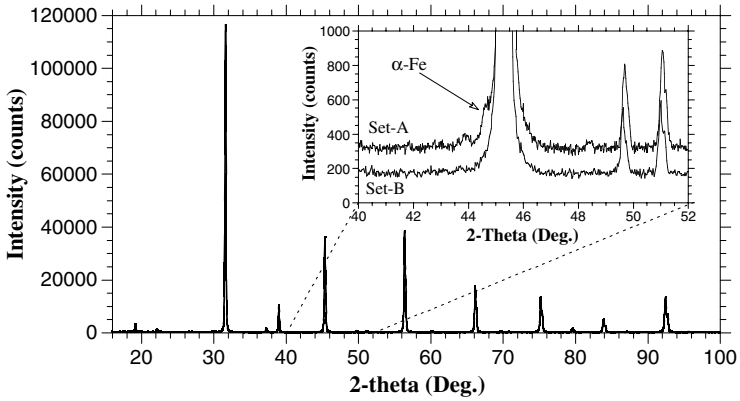

Figure 2. X-ray pattern at room temperature for $BaSrFeMoO_6$ (set-A) sample. Inset: detail of the x-ray pattern for both set of samples. Note that set A has been shifted upwards (100 counts) for the sake of clarity.

x-ray patterns considering two phases: double perovskite and α-Fe. The quantification gives less than 1% of the latter for all samples. It is noteworthy that this determination was not possible for Ba_2FeMoO_6 because the main peak of α-Fe coincides with the (4 0 0) structural peak of the double perovskite and the rest of the α-Fe peaks are barely detected in the pattern. Taking into account this result, we have performed a second analysis of A samples considering Fe–Fe scattering paths. The fit of the first-shell contribution is markedly improved by including the Fe–Fe contribution with an interatomic distance similar to that of α-Fe. We estimate 10% of Fe–Fe contribution to the first shell. This result should be taken carefully because EXAFS is not an accurate tool for quantitative analysis, but in this case the technique is very sensitive to α-Fe contamination due to the higher scattering factor of the Fe atom. Bearing in mind the atomic weights and coordination numbers of both phases, the weight ratio deduced from EXAFS analysis ranges between 1 and 1.5% in good agreement with the x-ray diffraction within the experimental error of both techniques. Nevertheless, the presence of amorphous Fe cannot be discarded to account for this small difference. Moreover, this finding could explain the Fe vacancies observed in the neutron refinements of these samples [3, 4].

An important result is that traces of α-Fe strongly affect the EXAFS analysis at the Fe K edge. Therefore, new synthesis routes were tested in order to minimize this undesirable effect. We were successful in preparing a set of samples free of α-Fe in their x-ray patterns (set B) with a softer reducing treatment (only 1 h). The inset of figure 2 compares the two samples of $BaSrFeMoO_6$ samples for instance. Moreover, the first-filtered-shell EXAFS spectra of B samples were perfectly fitted by considering only the oxygen coordination shell as can be seen in figure 1.

Finally, we have also verified that the new synthesis route does not affect the physical properties of these compounds. A comparison is summarized in table 1. As expected, there are minor changes in agreement with the presence of at least 98% of double perovskite in both kinds of samples. In some cases, the properties are improved as occurs with the saturated magnetization of Ba and $Ba_{1/2}Sr_{1/2}$ samples, closer to the theoretical value for set B. Therefore, hereafter we focus on the study of set B without significant impurities of α-Fe.

3.1.1. XANES spectra. Figure 3 shows the Fe K-edge XANES spectra at room temperature of A_2FeMoO_6, $LaFeO_3$ (as Fe^{3+} reference) and FeO (as Fe^{2+} reference). The spectra of

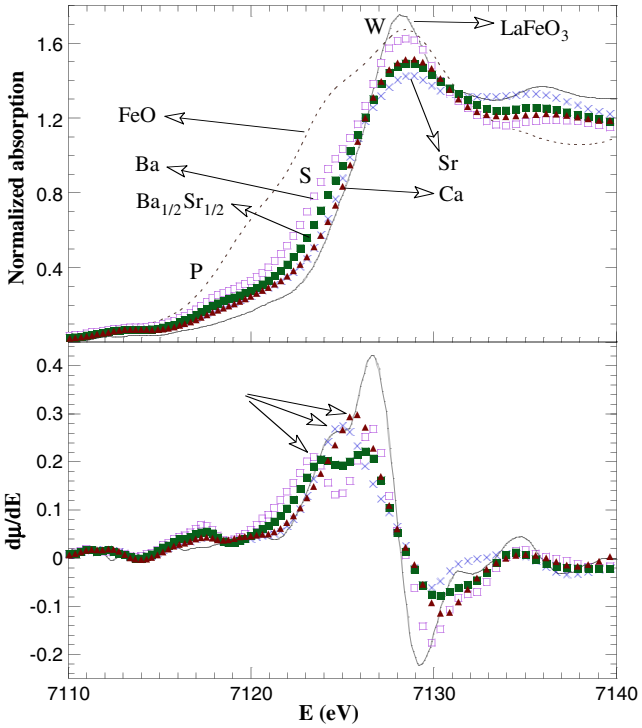

Figure 3. Top: XANES spectra of A_2FeMoO_6 samples at the Fe K absorption edge, A being Ba (open squares), $Ba_{1/2}Sr_{1/2}$ (solid squares), Sr (crosses) and Ca (triangles). The solid and dotted curves correspond to the references $LaFeO_3$ and FeO respectively. Bottom: the derivative near the absorption edge of the XANES spectra. Arrows indicate the first inflection point.

Table 1. Comparisons of lattice parameters, Curie temperature and saturated magnetic moment at 5 K for the samples indicated. A and B refer to the respective set of samples.

Sample	a (Å)	b (Å)	c (Å)	T_C (K)	M_S (μ_B/fu)
A–Ba_2FeMoO_6	8.0717(1)	—	—	308	3.53
B–Ba_2FeMoO_6	8.0686(1)	—	—	305	3.98
A–BaSrFeMoO$_6$	7.9799(1)	—	—	340	3.40
B–BaSrFeMoO$_6$	7.9745(1)	—	—	360	3.83
A–Sr_2FeMoO_6	5.5725(1)	—	7.8997(1)	385	2.95
B–Sr_2FeMoO_6	5.5704(1)	—	7.8924(1)	385	3.1
A–Ca_2FeMoO_6	5.4151(1)	5.5235(1)	7.7095(2)	365	3.5
B–Ca_2FeMoO_6	5.4165(1)	5.5238(1)	7.7170(2)	355	3.5

A_2FeMoO_6 samples are very similar to each other, as expected for the same crystallographic structure. A main resonance at the threshold (hereafter denoted as peak W), weak pre-peak structures (denoted as P) at ∼15 eV below peak W and a shoulder at intermediate energies between the previous features (denoted as S) can be seen. Features W and S correspond to dipolar transitions 1s → εp whose shape is related to the local geometrical structure. Differences among the spectra come from the different scattering powers of the divalent metals and may also be due to small differences in the crystal symmetry. The intensity W for A_2FeMoO_6 samples could be correlated with the change of symmetry in the series, from

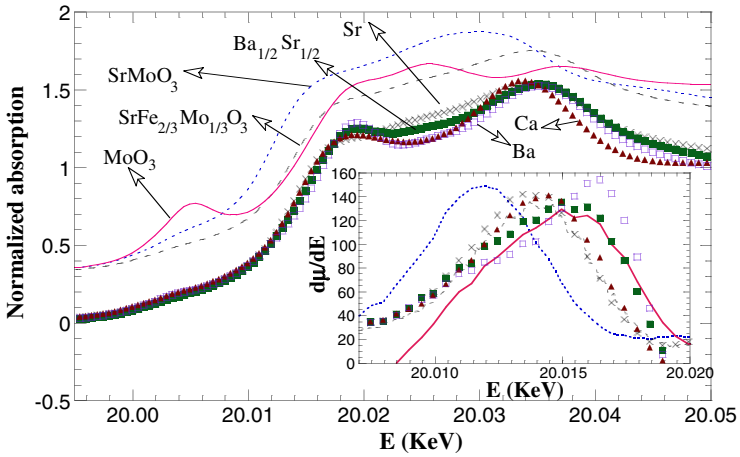

Figure 4. XANES spectra of the series A_2FeMoO_6 at the Mo K edge, where A is Ba (open squares), $Ba_{1/2}Sr_{1/2}$ (solid squares), Sr (crosses) and Ca (triangles). References are also plotted shifted upwards: the solid, dotted and broken curves correspond to MoO_3, $SrMoO_3$ and $SrFe_{2/3}Mo_{1/3}O_3$, respectively. The inset shows the derivative near the absorption edge of the XANES spectra.

cubic (Ba) to monoclinic (Ca) through tetragonal (Sr). P is ascribed to 1s $\rightarrow$ 3d transitions, either quadrupole allowed or dipole forbidden for an octahedral environment. The latter becomes allowed due to a strong mixing of O 2p and Fe 3d states. Some authors have claimed that the mixing of d states between different neighbouring transition metal atoms, through hybridization with the oxygen p band, gives rise to these pre-peaks [26]. Within this interpretation, the intensity of these pre-peaks would show a large mixing between 3d Fe and 4d Mo states. Curiously, this mixing seems not to exist between 3d Fe in the reference $LaFeO_3$. It is noteworthy that the shape of P features does not change significantly along the A_2FeMoO_6 series.

The main difference among the XANES spectra concerns to the energy position of the absorption edge. The edge position is mainly ascribed to the Fe oxidation state in this case. Different contributions from geometrical effects to the absorption edge position should be negligible due to the very similar crystallographic structure. The edges of $A_2FeMoO6$ samples are located close to the Fe^{3+} reference but an intermediate valence can be inferred for the Ba sample. In order to be more reliable, the derivative spectra are also shown in figure 3. The edge (taken as the first inflection) with the highest energy corresponds to $LaFeO_3$, the reference for octahedral Fe^{3+}. Ca_2FeMoO_6 and Sr_2FeMoO_6 have their edges at almost the same energy as the reference compound. Ba_2FeMoO_6 has the edge at the lowest energy whereas the value for $BaSrFeMoO_6$ is intermediate. Therefore, the maximum chemical shift is around 2 eV between the spectra of Ba and Ca samples. It is noteworthy that the chemical shift between Fe^{3+} and Fe^{2+} in our references is about 4 eV, a value in agreement with recent calculation [27]. Therefore, this finding may indicate an intermediate valence of the iron for Ba and $Ba_{1/2}Sr_{1/2}$ samples.

The Mo K-edge XANES spectra for A_2FeMoO_6 samples are plotted in figure 4 together with selected reference samples: MoO_3 (Mo^{6+}), $SrFe_{2/3}Mo_{1/3}O_3$ (Mo^{6+}-perovskite structure) and $SrMoO_3$ (Mo^{4+} perovskite structure). The Mo K-edge XANES of MoO_3 is characterized by a clear pre-peak at $\sim$12 eV below the absorption edge. Such a pre-peak has been reported in previous works as a shoulder of the main edge [28]. The better energy resolution of our experimental set-up allows us to discern a peak that arises from the distorted octahedral

coordination of α-MoO_3. The pre-peak transforms into a weak shoulder for the rest of the spectra in agreement with the nearly regular MoO_6 octahedra presented in either the double perovskites or the two other reference compounds.

The spectra of the double perovskites show a relatively weak white line and strong resonances above the edge related to multiple-scattering contributions (see figure 4). The Mo K edge of A_2FeMoO_6 samples lie very close to the Mo^{6+} references. However, the ascertainment of the Mo valence is more difficult here. First, the Mo K edge is broader than the Fe K edge. Second, this edge seems to be less susceptible to the chemical shift and small differences in the local structure have an important role. For instance the energy shift is $\sim$3.2 eV between α-MoO_3 and $SrMoO_3$ but only 1.7 eV between $SrFe_{2/3}Mo_{1/3}O_3$ and $SrMoO_3$. The difference between both Mo^{6+} references should be ascribed to the different geometrical environment and it is similar to the chemical shift between Mo^{4+} and Mo^{6+} in a perovskite structure. The inset of figure 4 displays the derivative of the absorption edges. It is clear that the double-perovskite curves peak at energies around the Mo^{6+} references. A mixed valence $+5\delta$ cannot be discounted for the Sr and Ca samples but, certainly, this is not the case for the Ba compound whose edge is located at the highest energy. In fact, a shift $\sim$2.5 eV is also observed along the series between the Ba sample and the Sr or Ca samples. This shift follows an opposite trend to that observed in the Fe K edge but this is only a qualitative comparison.

3.1.2. EXAFS spectra. Fe K-edge EXAFS spectra and the corresponding Fourier transform (FT) for A_2FeMoO_6 samples are shown in figure 5. The first oxygen coordination shells (first peaks of the FT) are alike for all samples but marked differences corresponding to the second-shell contribution (second peak of the FT) are detected. A small shift of the first peak position that indicates an increase of the interatomic Fe–O distances with increasing size of the alkaline-earth atom is noteworthy. Further peaks of the FT arise from different contributions: Fe–A, Fe–Mo distances and multiple-scattering paths such as Fe–O–O or Fe–O–Mo. The shape of these peaks strongly depends on each sample due to either the crystallographic symmetry or the different scattering power of the divalent cations. Intuitively, one would expect that the highest second peak corresponded to the most symmetrical environment, the cubic Ba_2FeMoO_6, that also shows the heaviest A atom (Ba) with a large scattering power. However, the strongest peak is found for the tetragonal Sr_2FeMoO_6 and it should be ascribed to phase shift effects from Fe–Ba paths. In this way, $BaSrFeMoO_6$ shows an intermediate behaviour. Finally, the monoclinic Ca_2FeMoO_6 shows weak broad peaks as expected for a broad distribution of interatomic distances. In order to confirm our interpretation, multiple-shell analysis, including both first and second shells, was used to analyse the EXAFS spectra up to $k \sim 14$ Å^{-1}. Figure 6 compares the imaginary part of the experimental FT spectra of Sr_2FeMoO_6 and Ca_2FeMoO_6 to the best-fit results using the FEFF 8.10 code. The accuracy of the fits confirms that spectral differences arise from the different scattering atoms presented in the second shell.

Taking into account that electronic properties mainly depend on the nearest neighbours, hereafter we are focusing on a first-shell analysis. The relevant parameters obtained from the FEFF analysis of the first shell between 1 and 2 Å are in good agreement with the crystallographic data [3]. Table 2 summarizes both Fe–O distances and Debye–Waller factors. The main result is that the Fe–O distance increases with increasing the size of atom A in agreement with the shift observed in the first peak of figure 5. Regular FeO_6 octahedral coordination is found for all samples with similar Debye–Waller factors.

EXAFS spectra at the Mo K edge and their FT are shown in figure 7. The first peak position of the FT is almost identical for all samples, showing that Mo–O interatomic distance does not depend on the divalent metal. As occurred at the Fe K edge, the main difference among the spectra corresponds to second-shell interatomic distances and also depends either

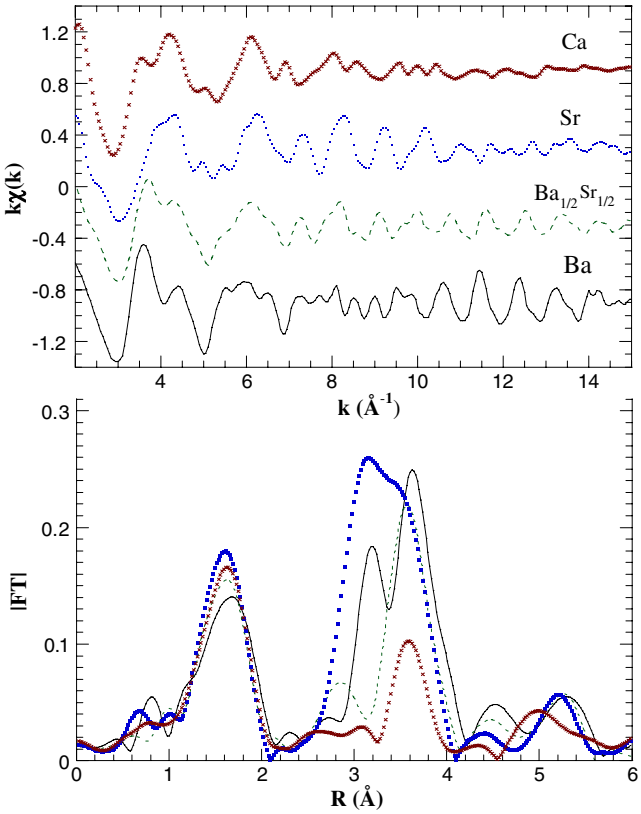

Figure 5. Top: EXAFS spectra, $k\chi(k)$, at the Fe K edge of A_2FeMoO_6 double perovskites, A being Ba (solid curve), $Ba_{1/2}Sr_{1/2}$ (dashed curve), Sr (dotted curve) or Ca (crosses). The spectra are shifted up or downwards for the sake of clarity. Bottom: their Fourier transforms that were extracted using a Gaussian window between 3.3 and 14 $Å^{-1}$.

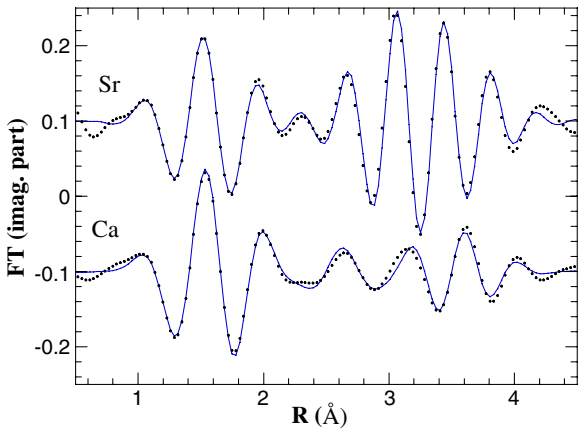

Figure 6. FT imaginary part and two-shell best fit of Sr_2FeMoO_6 (top) and Ca_2FeMoO_6 (bottom) K-edge EXAFS spectra. The spectra are shifted (±0.1) for the sake of clarity.

on the crystallographic symmetry or on the different scattering powers of the divalent cations. In this case, the most symmetrical structure, the cubic Ba_2FeMoO_6, presents a strong second peak at the Mo K edge corresponding to a narrow distribution of Mo–Ba distances.

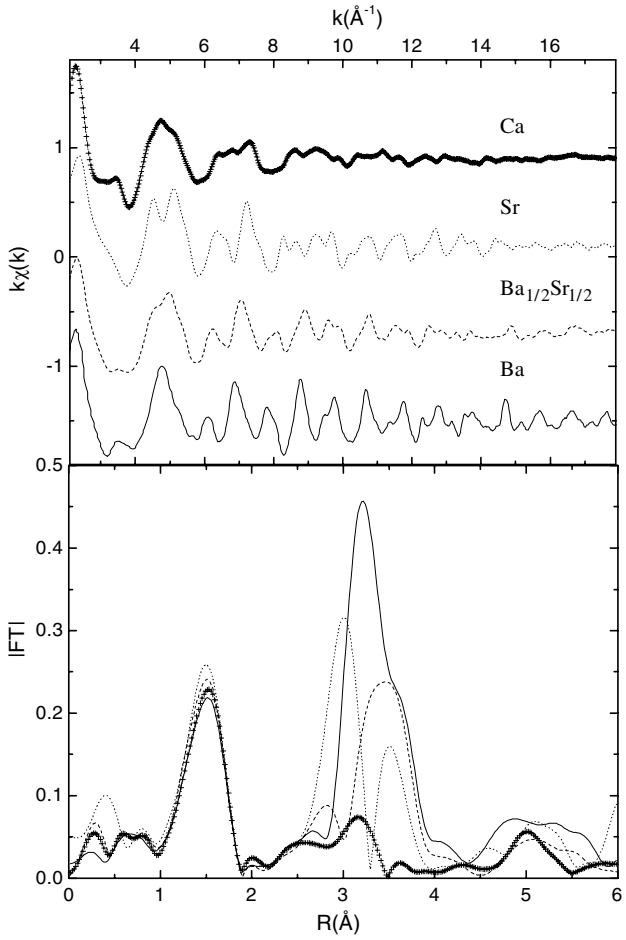

Figure 7. Top: EXAFS spectra ($k\chi(k)$) at the Mo K edge of A_2FeMoO_6 double perovskites, A being Ba (solid curve), $Ba_{1/2}Sr_{1/2}$ (dashed curve), Sr (dotted curve) or Ca (crosses). Bottom: their Fourier transforms that were extracted using a Gaussian window between 3 and 18 Å^{-1}.

Table 2. Distances r[Fe(Mo)–O] and Debye–Waller factors σ obtained with the FEFF 8.0 code for the A_2FeMoO_6 samples at 30 K. Coordination number and ΔE_0 have been fixed to six and zero, respectively, for all fits considered. Numbers in parenthesis refer to standard deviations of the last significant digit.

	Fe K edge		Mo K edge	
Sample (A)	$\langle r \rangle$	$\langle \sigma^2 \rangle$	$\langle r \rangle$	$\langle \sigma^2 \rangle$
Ba_2FeMoO_6	2.080(5)	0.005(1)	1.960(6)	0.002(1)
$BaSrFeMoO_6$	2.030(6)	0.004(1)	1.950(7)	0.002(1)
Sr_2FeMoO_6	2.000(5)	0.004(1)	1.960(6)	0.002(1)
Ca_2FeMoO_6	2.020(5)	0.004(1)	1.950(5)	0.002(1)

The first-shell contribution at the Mo K edge was extracted by Fourier filtering of the FT spectra between 0.9 and 1.9 Å. The Mo–O distances and Debye–Waller factors were the only fitting parameters. The best-fit results are also summarized in table 2. The data seem to be quite reasonable with minor changes in the Mo–O values that also agree with those reported from crystallographic studies [3, 4]. The Debye–Waller factors also point to the presence of regular MoO_6 octahedra.

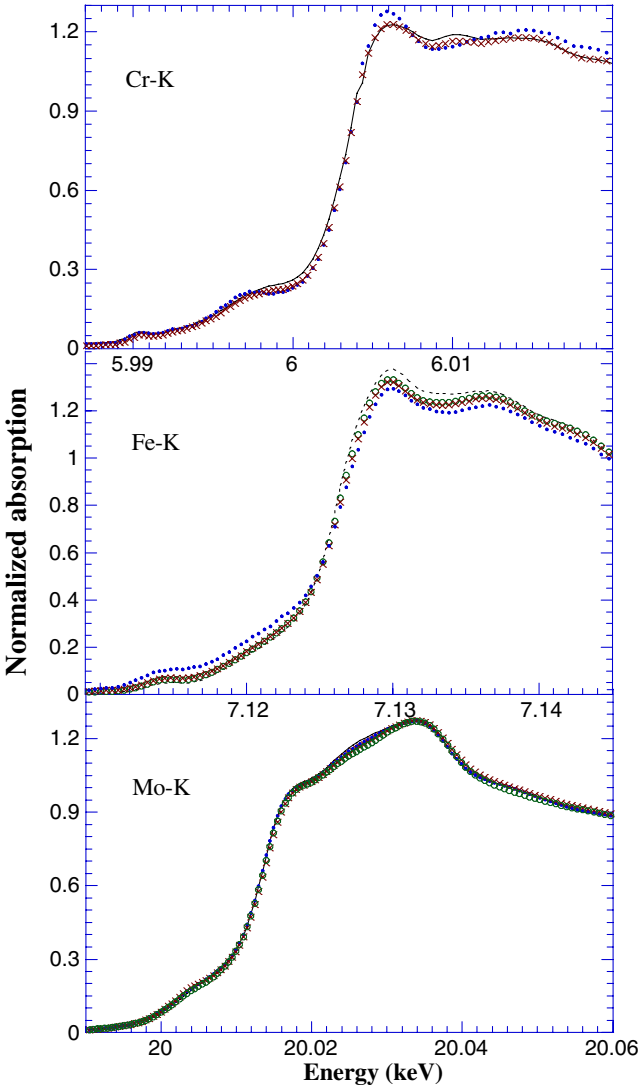

Figure 8. XANES spectra of the $Sr_2Fe_{1-x}Cr_xMoO_6$ samples at the Cr, Fe and Mo K edges. Solid curve, points, crosses, circles and dotted curve refer to $x = 1$, 0.75, 0.50, 0.25 and 0, respectively. The data were collected at 30 K.

3.2. $Sr_2Fe_{1-x}Cr_xMoO_6$ series

We have observed the strong influence of A atoms in the electronic properties of the B sublattice. Now, the A atom (Sr) is fixed and we replace Fe by Cr in the lattice in order to check the effects on Fe and Mo atoms. It is well known that Cr^{3+} is the most stable oxidation state in related perovskite oxides so the present study allows us to gain insight into the electronic state of Mo atoms.

The XANES spectra of selected $Sr_2Fe_{1-x}Cr_xMoO_6$ samples at the Cr, Fe and Mo K edges are shown in figure 8. No significant differences among the XANES spectra of each particular edge were observed. The differences in the edge position are less than 0.5 eV among all the samples for each K edge, suggesting no changes in the oxidation state of the three atoms along the series. The comparison of the edge position with the respective references $LaCrO_3$ (or $LaFeO_3$) certifies that the Cr (or Fe) oxidation state is closely to +3. Therefore, the substitution of Fe with Cr is homovalent. This replacement also seems not to affect the Mo valence.

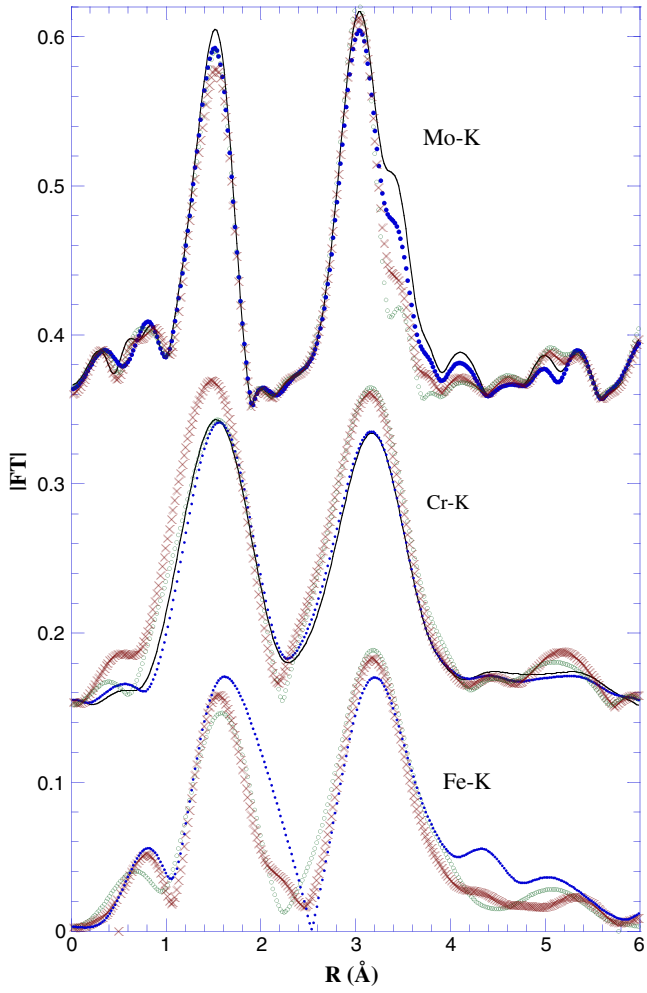

Figure 9. FT spectra of $Sr_2Fe_{1-x}Cr_xMoO_6$ samples at the Mo K edge (top), Cr K edge (middle) and Fe K edge (bottom) for $x = 0.25$ (squares), 0.5 (crosses), 0.75 (points) and 1 (solid curve). The data were taken at 30 K.

The EXAFS spectra of the $Sr_2Fe_{1-x}Cr_xMoO_6$ samples ($1/4 \leqslant x \leqslant 3/4$) were also analysed using the FEFF 8.10 code. The FT of the $k\chi(k)$ spectra was extracted using a Gaussian window between 3 and 18 Å^{-1} for the Mo K edge and between 4.5 and 11 Å^{-1} for the Fe and Cr K edges. The short k-range for the latter edges is conditioned by the energy range of the EXAFS signal that can be analysed in terms of signal/noise ratio (due to either dilution or low energy of Cr K edge). The comparison of our results with the crystallographic data ensures the accuracy of our analysis. The FT spectra for all edges are plotted in figure 9. The FT spectra show two well defined peaks corresponding to the two nearest coordination shells around the central atom. The position of the first peak in the Mo spectra (Mo–O distance) is the same for all the studied samples, indicating a similar MoO_6 octahedron when Cr replaces Fe in the lattice. The second peak shows a shoulder at high R that increases as the content of Cr does. The FT spectra of both Fe and Cr K edges also show minor changes with x. The first-shell contribution was extracted by Fourier filtering of the FT spectra between 0.8 and 2.3 Å at the Fe(Cr) K edge and between 0.9 and 1.9 Å at the Mo K edge. The best-fit results are summarized in the table 3. The data reasonably agree with the crystallographic data [19] and with the tabulated ionic radii [18]. We did not observe noticeable changes in any of the

Table 3. Distances r [Mo(Cr, Fe)–O] and Debye–Waller factors σ for the $Sr_2Fe_{1-x}Cr_xMoO_6$ series at 30 K. The coordination number and ΔE_0 have been fixed to six and zero, respectively, for all fits considered. Numbers in parenthesis refer to standard deviations of the last significant digit.

	Mo K edge		Fe K edge		Cr K edge	
Sample	$\langle r \rangle$	$\langle \sigma^2 \rangle$	$\langle r \rangle$	$\langle \sigma^2 \rangle$	$\langle r \rangle$	$\langle \sigma^2 \rangle$
$Sr_2Fe_{3/4}Cr_{1/4}MoO_6$	1.960(7)	0.002(1)	1.990(7)	0.005(1)	1.980(12)	0.002(1)
$Sr_2Fe_{1/2}Cr_{1/2}MoO_6$	1.950(4)	0.002(1)	1.990(7)	0.005(1)	1.950(6)	0.002(1)
$Sr_2Fe_{1/4}Cr_{3/4}MoO_6$	1.960(5)	0.002(1)	1.990(9)	0.004(1)	1.980(3)	0.002(1)
Sr_2CrMoO_6	1.950(5)	0.002(1)	—	—	1.970(3)	0.002(1)

interatomic distances along the $Sr_2Fe_{1-x}Cr_xMoO_6$ series. This agrees with the absence of changes in the XANES spectra.

4. Discussion and conclusions

The description of the oxidation state of molybdenum and iron in A_2FeMoO_6 double perovskites is nowadays a matter of controversy. This work adds a new factor to gain insight into the understanding of these compounds. The electronic structure of the B sublattice depends on the alkaline-earth partner. First of all, there is no unique ionic approximation suitable to describe the properties of the whole series. XANES spectra suggest a valence state for Fe ranging between 3+ (Sr and Ca) and 2.5+ (Ba) whereas the valence for Mo cannot be determined unambiguously between $Mo^{5-\delta+}$ and Mo^{6+}. For Ca and Sr compounds, the EXAFS spectra gave interatomic distances (see table 2) that correlate quite well [18] to the theoretical values of Fe^{3+}(HS)–O (∼2.01 Å) and Mo^{5+}–O (1.97 Å). However the ionic model fails to describe the Ba compound whose Fe K-edge XANES suggests a mixed valence, and the Mo K-edge XANES evidences the highest oxidation state for Mo. In this way, the interatomic Fe–O distance is intermediate between Fe^{3+}(HS)–O and Fe^{2+}(HS)–O (∼2.14 Å) in agreement with the XANES result. Finally, the $Ba_{1/2}Sr_{1/2}$ compound shows an intermediate behaviour between the former samples. This sequence is also observed in other measurements. Neutron diffraction refined a localized magnetic moment on the Mo site in Ca and Sr samples (Mo^{5+} or $4d^1$ as a rough approximation) whereas no significant moment was detected for Ba or $Ba_{1/2}Sr_{1/2}$ compounds (Mo^{6+}, $5d^0$). Nevertheless, there is no Fe^{2+} in the latter compounds so an ionic picture seems to be meaningless to describe this series as occurs in related systems [29]. According to Szotek *et al* [11], valence is defined as the integer number of electrons available for band formation. Therefore, the nominal valence band in the ground state would be Fe^{3+} and Mo^{6+}, regarding the SIC-LSD calculation [11]. The electron in the conduction band is antiferromagnetically coupled to the localized Fe^{3+} moments. This scenario is similar to that given by Sarma *et al* [12], who considered a localized Fe 3d band (Fe^{3+}: $3d^5$) and an electron delocalized on the Mo 4d band (Mo^{5+}: $4d^1$). Anyway, the electronic and spin density projection on either Fe^{3+} (Ba and $Ba_{1/2}Sr_{1/2}$) or Mo^{6+} (Sr, Ca) sites will highly depend on the type of A atom as demonstrated by our work. It may also depend on the synthesis details explaining the differences reported in the spectroscopic measurements of Sr_2FeMoO_6 [12–16].

The study of the $Sr_2Fe_{1-x}Cr_xMoO_6$ series brings forward new keys in the understanding of this system. The oxidation state for Fe and Cr is +3 for all samples so the substitution is homovalent. We have not detected any noticeable change in the electronic state of Mo ions along the series. This is true even though Sr_2CrMoO_6 presents a large number of oxygen vacancies. Therefore, the existence of Mo^{6+} or Mo^{5+} could be meaningless because the

covalence between these ions and oxygen is very strong and the hole may be mainly located on the oxygen atoms. Then, it is hard to differentiate between Mo^{5+} and Mo^{6+} in the Mo K-edge XANES. Therefore, the metal–insulator transition observed in the $Sr_2Fe_{1-x}Cr_xMoO_6$ series with increasing x cannot be attributed to a change in the transition-metal electronic state but to further effects such as oxygen vacancies or miss-site disorder.

Acknowledgments

We acknowledge the financial support from the Spanish CICyT MAT02-01221 project and from DGA. We thank ESRF for granting beam time and BM29 staff for help in performing the experiment.

References

[1] Kobayashi K-I, Kimura T, Sawada H, Terakura K and Tokura Y 1998 *Nature* **395** 677
[2] Galasso F, Douglas F C and Kasper R 1966 *J. Chem. Phys.* **44** 1672
[3] Ritter C, Ibarra M R, Morellon L, Blasco J, Garcia J and De Teresa J M 2000 *J. Phys.: Condens. Matter* **12** 8295
[4] Chmaissem O, Kruk R, Dabrowski B, Brown D E, Xiong X, Kolesnik S, Jorgensen J D and Dimball C W 2000 *Phys. Rev.* B **62** 14197
[5] Alonso J A, Casais M T, Martínez-Lopez M J, Martínez J L, Velasco P, Muñoz A and Fernández-Díaz M T 2000 *Chem. Mater.* **12** 161
[6] Alamelu T, Varadaraju U V, Venkatesan M, Douvalis A P and Coey J M D 2002 *J. Appl. Phys.* **91** 8909
[7] Fang Z, Terakura K and Kanamori J 2001 *Phys. Rev.* B **63** 180407
[8] Navarro J, Balcells Ll, Sandiumenge F, Bibes M, Roig A, Martínez B and Fontcuberta J 2001 *J. Phys.: Condens. Matter* **13** 8481
[9] Patterson F K, Moeller C W and Ward R 1962 *Inorg. Chem.* **1** 196
[10] Longo L and Wald R 1961 *J. Am. Chem. Soc.* **83** 2816
[11] Szotek Z, Temmerman W M, Svane A, Petit L and Winter H 2003 *Phys. Rev.* B **68** 104411
[12] Sarma D D, Mahadevan P, Sha-Dasgupta T, Ray S and Kumar A 2000 *Phys. Rev. Lett.* **85** 2549
[13] Ray S, Kumar A, Sarma D D, Cimino R, Turchini S, Zennaro S and Zema N 2001 *Phys. Rev. Lett.* **87** 097204
[14] Besse M, Cros V, Barthelemy A, Jaffres H, Vogel J, Petroff F, Mirone A, Tagliaferri A, Bencok P, Decorse P, Berthet P, Szotek Z, Temmerman W M, Dhesi S S, Brookes N B, Rogalev A and Fert A 2002 *Europhys. Lett.* **60** 608
[15] Moreno M S, Goyane J E, Abbate M, Caneiro A, Niebieskikwiat D, Sánchez R D, de Siervo A, Landers R and Zampieri G 2001 *Solid State Commun.* **120** 161
[16] Sarma D D, Sampathkumaran E V, Ray S, Nagarajan R, Majumdar S, Kumar A, Nalini G and Guru Row T N 2000 *Solid State Commun.* **114** 465
[17] Balcells Ll, Navarro J, Bibes M, Roig A, Martínez B and Fontcuberta J 2001 *Appl. Phys. Lett.* **78** 781
[18] Shannon R D 1976 *Acta Crystallogr.* A **32** 751
[19] Blasco J, Ritter C, Morellón L, Algarabel P A, De Teresa J M, Serrate D, García J and Ibarra M R 2002 *Solid State Sci.* **4** 651
[20] Arulraj A, Ramesha K, Gopalakrishnan J and Rao C N R 2000 *J. Solid State Chem.* **155** 233
[21] Kim B G, Hor Y-S and Cheong S-W 2001 *Appl. Phys. Lett.* **79** 338
[22] Navarro J, Frontera C, Balcells Ll, Martínez B and Fontcuberta J 2001 *Phys. Rev.* B **64** 092411
[23] Kang J-S, Han H, Lee B W, Olson C G, Han S W, Kim K H, Jeong J I, Park J H and Min B I 2001 *Phys. Rev.* B **64** 024429
[24] Koningsberger D C and Prins R 1988 *X-ray Absorption: Principles, Application, Techniques of EXAFS, SEXAFS and XANES* (New York: Wiley)
[25] Stern E A, Newville H, Ravel B, Yaroby Y and Haskel D 1995 *Physica* B **208/209** 117 http://FEFF.phys.washington.edu/
[26] Joly Y, Cabaret D, Renevier H and Natoli C R 1999 *Phys. Rev. Lett.* **82** 2398
[27] Benfatto M, Solera J A, García J and Chaboy J 2002 *Chem. Phys.* **282** 441
[28] Kuzmin A and Purans J 2000 *J. Phys.: Condens. Matter* **12** 1959
[29] García J, Blasco J, Sánchez M C, Proietti M G and Subías G 2002 *Surf. Rev. Lett.* **9** 821